

Article

Resonant Converter with Soft Switching and Wide Voltage Operation

Bor-Ren Lin 

Department of Electrical Engineering, NYUST, Yunlin 640, Taiwan; linbr@yuntech.edu.tw; Tel.: +886-912312281

Received: 25 July 2019; Accepted: 8 September 2019; Published: 9 September 2019



Abstract: A new DC/DC resonant converter with wide output voltage range operation is presented and studied to have the benefits of low switching losses on active devices and low voltage stresses on power diodes. To overcome serious reverse recovery losses of power diodes on a conventional full-bridge pulse-width modulation converter, the resonant converter is adopted to reduce the switching loss and increase the circuit efficiency. To extend the output voltage range in conventional half-bridge or full-bridge resonant converters, the secondary sides of two diode rectifiers are connected in series to have wide output voltage operation. The proposed converter can be either operated at one-resonant-converter mode for low voltage range or two-resonant-converter mode for high voltage range. Thus, the voltage rating of power diodes is decreased. Experiments with the design example are given to show the circuit performance and validate the theoretical discussion and analysis.

Keywords: low soft switching; reverse recovery current loss; wide output voltage range

1. Introduction

Power saving and power loss issues have become more and more important with respect to reducing the effect of global warming. Low power loss means less power demand is needed from the utility company. Modern power converters have demanded the development of high power density and low power loss for modern consumer and industry products. Soft switching techniques or wide-band gap power devices, such as SiC or GaN power switches, have been widely developed to lessen the switching losses. SiC and GaN have low switching loss characteristics and power converters and can operate at high frequency and high power density, however, the wide-band gap power switches are much more expensive than the conventional MOSFETs. For zero voltage switching techniques, a quasi-resonant (QR) approach has been applied in flyback [1,2] to lessen the switching loss. The circuit efficiency of QR flyback with synchronous rectifier can be higher than 90%. Active clamp techniques [3] have been applied in buck, boost, flyback, and forward converters to lessen the switching losses for low-power applications. More components are needed in the circuit, and these additional components introduce more power loss. For medium-power products, resonant converters [4–7] and full-bridge pulse width modulation converters [8–11] were developed to reduce switching losses. Full-bridge converters lose soft switching operation at low output power and the circuit efficiency will decrease at low load conditions. The resonant converters have soft switching characteristics on power semiconductors over the full load range so that the efficiency of the resonant converter at low load is better than phase-shift full-bridge converters. The limited voltage variation range is the main drawback of the resonant converters. If the voltage operation range is increased, then the low inductor ratio and low quality factor should be used. However, the circulating current and conduction loss on the primary side will increase and the circuit efficiency decreases.

Wide output voltage power converters are demanded for battery chargers for hybrid electric vehicles or outdoor LED lighting systems. In electric vehicle and hybrid electric vehicle battery charging systems, the single-phase power factor corrector and isolated DC converter are used in type I and II

charging systems, and the three-phase power factor corrector and full-bridge DC converter are adopted in type III charging system. The output voltage of the high-voltage battery stack in PHEV and EV varies widely with battery capacity, such as 200–420 V. In outdoor LED lighting systems, the DC output voltage is variable for different series and parallel combinations of LED strings' applications, such as 120–360 V. The DC-DC converters with wide output voltage variation have been developed for battery chargers. To achieve wide output voltage capability, the full-bridge DC converters with phase-shift pulse width modulation were presented and discussed in [12,13] to have high circuit efficiency and low switching losses. The voltage range is limited to less than 2:1 ($v_{o,max} = 2v_{o,min}$) or 3:1 ($v_{o,max} = 3v_{o,min}$) due to low converter efficiency in low duty cycle or low output voltage cases. To realize a wide output voltage range, the basic circuit topologies are two-stage DC-DC converters (boost or buck converter + full-bridge converter) to implement 4:1 ($v_{o,max} = 4v_{o,min}$) voltage variation. However, the circuit efficiency is reduced in these circuit topologies. The hybrid resonant converter with half-bridge or full-bridge operation has been studied in [14–16] to increase the voltage operation range, such as a 4:1 voltage range, $v_{in,max} = 4v_{in,min}$. The main problems are that a transient operation interval will be introduced between the half-bridge resonant circuit and the full-bridge resonant circuit operation, and one power switch is always conducting under the half-bridge resonant circuit to decrease circuit efficiency. The voltage rating of power diodes on conventional full-bridge or center-tapped diode rectifiers equals the output voltage or two times the output voltage, respectively. The rectifier diodes have serious voltage stress problems for high-voltage output conditions.

A hybrid resonant circuit with an input-parallel output-series structure is presented and studied to accomplish the improvements of the low-voltage rating on power diodes, wide voltage operation range, and wide soft switching range. By using the frequency modulation approach, the proposed converter is controlled under inductive impedance. The soft switching operation of power devices is achieved. The switching losses on power semiconductors are reduced. To overcome the high-voltage rating problem on rectifier diodes, two full-bridge diode rectifiers are employed on the proposed circuit. For high-voltage output, two full-bridge resonant converters are all operated and the secondary-side rectified voltages are series-connected. The voltage rating of each diode is $V_{o,H}/2$ instead of $V_{o,H}$ in conventional DC-DC converters. On the other hand, only one full-bridge resonant converter is operated under the low-voltage output case. Only one diode rectifier is connected to the output load and the other diode rectifier is bypassed. The voltage rating of the power diodes is $V_{o,L}$. The drawback of the high-voltage rating on rectifier diodes is improved in the presented circuit. The theoretical analysis, the principle of operation, and the design procedure are provided in this paper. Finally, a 2 kW laboratory circuit was built and tested. Experimental results are used to confirm the theoretical analysis and demonstrate the helpfulness of the presented hybrid resonant converter for wide output voltage capability.

2. Circuit Structure and Operating Principle

The studied converter with wide output voltage operation is illustrated in Figure 1a. Two resonant converters with primary-parallel secondary-series connection are adopted to accomplish the wide voltage operation. V_{in} is the input voltage. V_o is the output voltage. In each DC converter, the primary side is a full-bridge resonant structure and the secondary side is the full-bridge diode rectifier. Four power switches are used in the full-bridge resonant structure and four rectifier diodes are employed in the full-bridge rectifier structure. C_{r1} and L_{r1} are naturally resonant in circuit 1 and C_{r2} and L_{r2} are resonant in circuit 2. For high-voltage output, two converters are operated and V_o is the summation of the rectified voltages of two full-bridge diode rectifiers shown in Figure 1a. For low-voltage output (Figure 1b), only converter 1 ($S_1 \sim S_4$) is controlled and converter 2 ($S_5 \sim S_8$) is off. The load voltage V_o equals the rectified voltage of the full-bridge rectifier by $D_1 \sim D_4$ and the diodes $D_5 \sim D_8$ are forward-biased to bypass the secondary side current of transformer T_1 . The wide output voltage is achieved in the studied circuit. The frequency control method is adopted to control active devices and

adjust the load voltage. The power semiconductors are operated with soft switching characteristics due to the resonant tank having an inductive impedance characteristic.

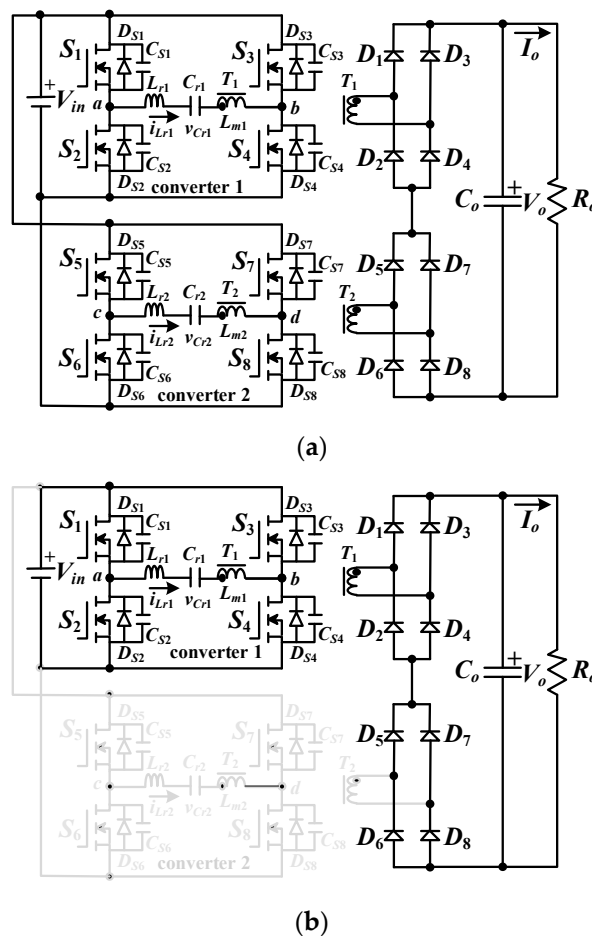


Figure 1. Circuit configuration of the studied circuit (a) for high-voltage output operation, and (b) for low-voltage output operation.

2.1. High-Voltage Output

The resonant converter is controlled by the frequency modulation. If f_s (the switching period) $>$ or $<$ f_r (series resonant frequency), there are four or six operating modes in every switching period. For high output voltage range, two converters are controlled to increase the load voltage due to the series connection of two full-bridge diode rectifiers at the load side, as shown in Figure 1a. Figure 2a (Figure 2b) illustrates the voltage and current waveforms of the studied converter at high-voltage output under $f_s > f_r$ ($f_s < f_r$) condition. Figure 2c–h demonstrate six equivalent mode circuits at high-voltage output operation and $f_s < f_r$ (Figure 2b). If $f_s > f_r$ (Figure 2a), only modes 1, 3, 4, and 6 are operated in a switching cycle.

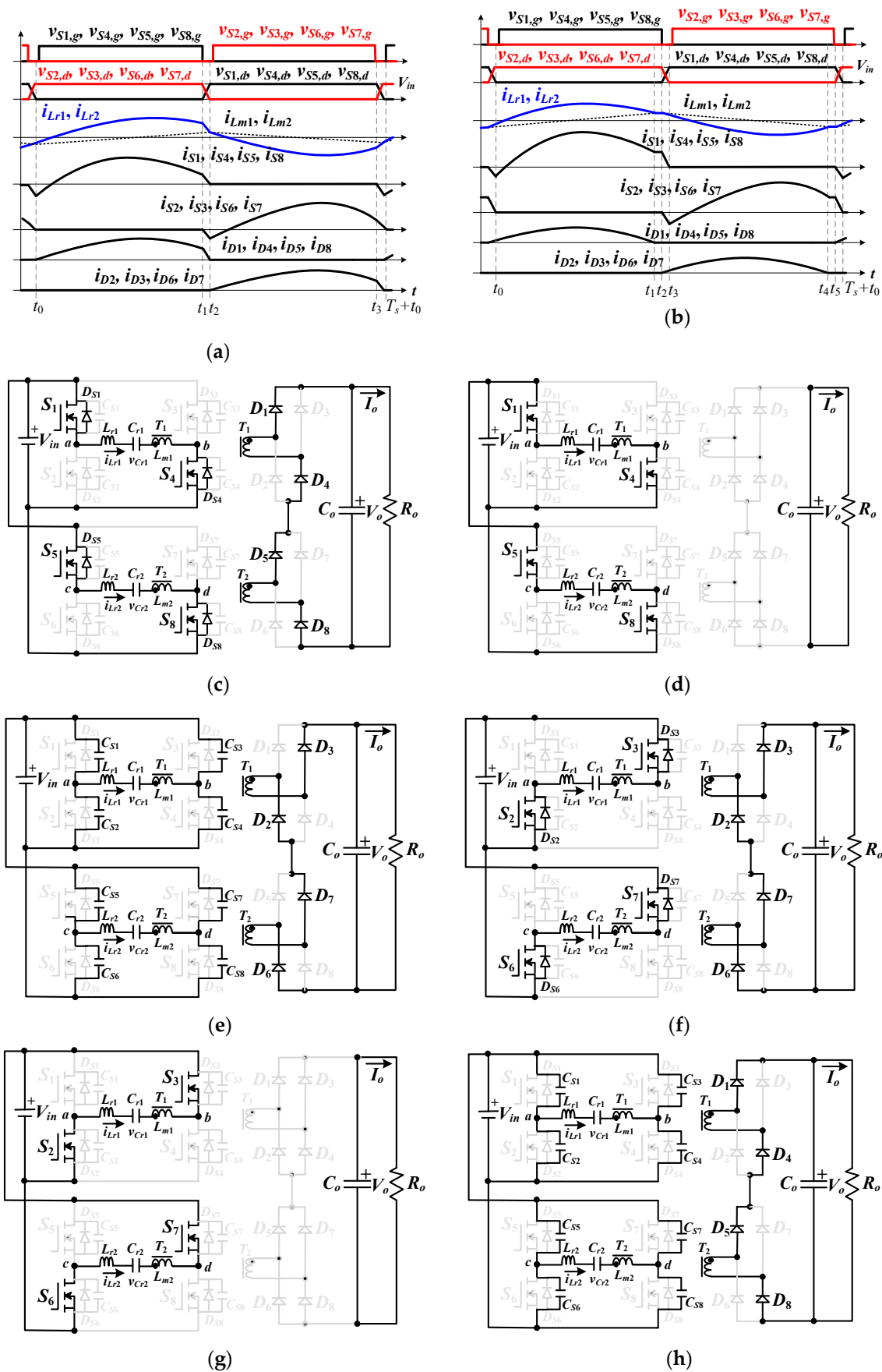


Figure 2. Circuit waveforms and equivalent mode circuits at high-voltage output. (a) PWM waveforms when $f_s > f_r$; (b) PWM waveforms when $f_s < f_r$; (c) mode 1; (d) mode 2; (e) mode 3; (f) mode 4; (g) mode 5; and (h) mode 6.

Mode 1 [t_0, t_1]: At time $t < t_0$, $S_1 \sim S_8$ are off and i_{Lr1} and i_{Lr2} are negative. C_{S1}, C_{S4}, C_{S5} , and C_{S8} are discharged and C_{S2}, C_{S3}, C_{S6} , and C_{S7} are charged. At t_0 , $v_{CS1} = v_{CS4} = v_{CS5} = v_{CS8} = 0$. Since $i_{Lr1}(t_0)$ and $i_{Lr2}(t_0)$ are all negative value, D_{S1}, D_{S4}, D_{S5} , and D_{S8} are conducting. S_1, S_4, S_5 , and S_8 turn on after t_0 under zero voltage. Due to D_1, D_4, D_5 , and D_8 are conducting, $v_{Lm1} = v_{Lm2} = nV_o/2$ where n is the turns ratio of T_1 and T_2 . C_{r1} and L_{r1} are naturally resonant in converter 1 and C_{r2} and L_{r2} are resonant in converter 2 with $v_{ab} = v_{cd} = V_{in}$ and $v_{Lm1} = v_{Lm2} = nV_o/2$. The series resonant frequency in mode 1 is $f_r = 1/2\pi\sqrt{L_{r1}C_{r1}}$. If $f_s < f_r$, then i_{D1}, i_{D4}, i_{D5} , and i_{D8} will be decreased to zero current before S_1, S_4, S_5 , and S_8 turn off.

Mode 2 [t_1, t_2]: Owing to $f_s < f_r$, $i_{Lm1}(t_1) = i_{Lr1}(t_1)$ and $i_{Lm2}(t_1) = i_{Lr2}(t_1)$ so that $i_{D1} = i_{D4} = i_{D5} = i_{D8} = 0$. No power is delivered to the load resistor. (L_{m1}, L_{r1} , and C_{r1}) and (L_{m2}, L_{r2} , and C_{r2}) are resonant with input voltage $v_{ab} = v_{cd} = V_{in}$ in converters 1 and 2, respectively.

Mode 3 [t_2, t_3]: S_1, S_4, S_5 and S_8 turn off at t_2 . C_{S2}, C_{S3}, C_{S6} , and C_{S7} are discharged in mode 2 due to $i_{Lr1}(t_2) > 0$ and $i_{Lr2}(t_2) > 0$. Since the secondary side currents of T_1 and T_2 are negative, the diodes D_2, D_3, D_6 , and D_7 conduct. If the energy stored on (L_{r1} and L_{m1}) and (L_{r2} and L_{m2}) at time t_2 is large enough, then the voltages of C_{S2}, C_{S3}, C_{S6} and C_{S7} are decreased to zero at $t = t_3$. The resonant currents are calculated in Equation (1):

$$i_{Lr1}(t_2) = i_{Lr2}(t_2) \geq i_{Lm1}(t_2) = i_{Lm2}(t_2) = nV_o/(4L_m f_s) \quad (1)$$

where $L_m = L_{m1} = L_{m2}$. The soft switching condition of S_2, S_3, S_6 , and S_7 are given in Equation (2):

$$i_{Lm1}(t_2) = i_{Lm2}(t_2) \geq V_{in} \sqrt{4C_e/(L_m + L_r)} \quad (2)$$

where $C_e = C_{S1} = \dots = C_{S8}$ and $L_r = L_{r1} = L_{r2}$. If the dead time t_d between each switch is given, then the maximum magnetizing inductances are calculated in Equation (3):

$$L_{m1} = L_{m2} \leq \frac{nV_o t_d}{8V_{in} f_s C_e} \quad (3)$$

Mode 4 [t_3, t_4]: The voltages of C_{S2}, C_{S3}, C_{S6} , and C_{S7} are reduced to zero at t_3 . D_{S2}, D_{S3}, D_{S6} , and D_{S7} are forward biased owing to $i_{Lr1}(t_3)$ and $i_{Lr2}(t_3)$ are positive value. S_2, S_3, S_6 , and S_7 turn on after t_3 with zero voltage condition. In mode 4, D_2, D_3, D_6 , and D_7 are conducting so that $v_{Lm1} = v_{Lm2} = -nV_o/2$. (C_{r1} and L_{r1}) and (C_{r2} and L_{r2}) are naturally resonant in converters 1 and 2, respectively, with input voltage $v_{ab} = v_{cd} = -V_{in}$ and load voltage $v_{Lm1} = v_{Lm2} = -nV_o/2$. If $f_s < f_r$, then i_{D2}, i_{D3}, i_{D6} , and i_{D7} will be decreased to zero current before S_2, S_3, S_6 , and S_7 are turned off.

Mode 5 [t_4, t_5]: Since $f_s < f_r$, $i_{Lm1} = i_{Lr1}$ and $i_{Lm2} = i_{Lr2}$ at time t_4 and $i_{D2} = i_{D3} = i_{D6} = i_{D7} = 0$. No power is transferred to the load resistor. (L_{m1}, L_{r1} and C_{r1}) and (L_{m2}, L_{r2} and C_{r2}) are naturally resonant in converters 1 and 2, respectively, with input voltage $v_{ab} = v_{cd} = -V_{in}$.

Mode 6 [$t_5, T_s + t_0$]: At t_5 , S_2, S_3, S_6 , and S_7 turn off. Due to $i_{Lr1}(t_5)$ and $i_{Lr2}(t_5)$ are negative value, C_{S1}, C_{S4}, C_{S5} , and C_{S8} are discharged. At time $T_s + t_0$, the voltages of C_{S1}, C_{S4}, C_{S5} , and C_{S8} are decreased to zero voltage and the studied circuit goes to the next switching cycle operation.

2.2. Low-Voltage Output

For low-voltage output, only $S_1 \sim S_4$ are controlled and $S_5 \sim S_8$ are off. The secondary side voltage of T_1 is connected to the output load and $D_5 \sim D_8$ are forward biased, as shown in Figure 1b. Figure 3a,b give the current and voltage waveforms of the studied circuit for low-voltage output under $f_s > f_r$ and $f_s < f_r$ conditions, respectively. If $f_s > f_r$ (Figure 3a), only modes 1, 3, 4, and 6 are operated in a switching cycle. If $f_s < f_r$ (Figure 3b), there are six equivalent mode circuits (Figure 3c–h) at low-voltage output operation. The operation principle at low-voltage output at $f_s < f_r$ is presented below.

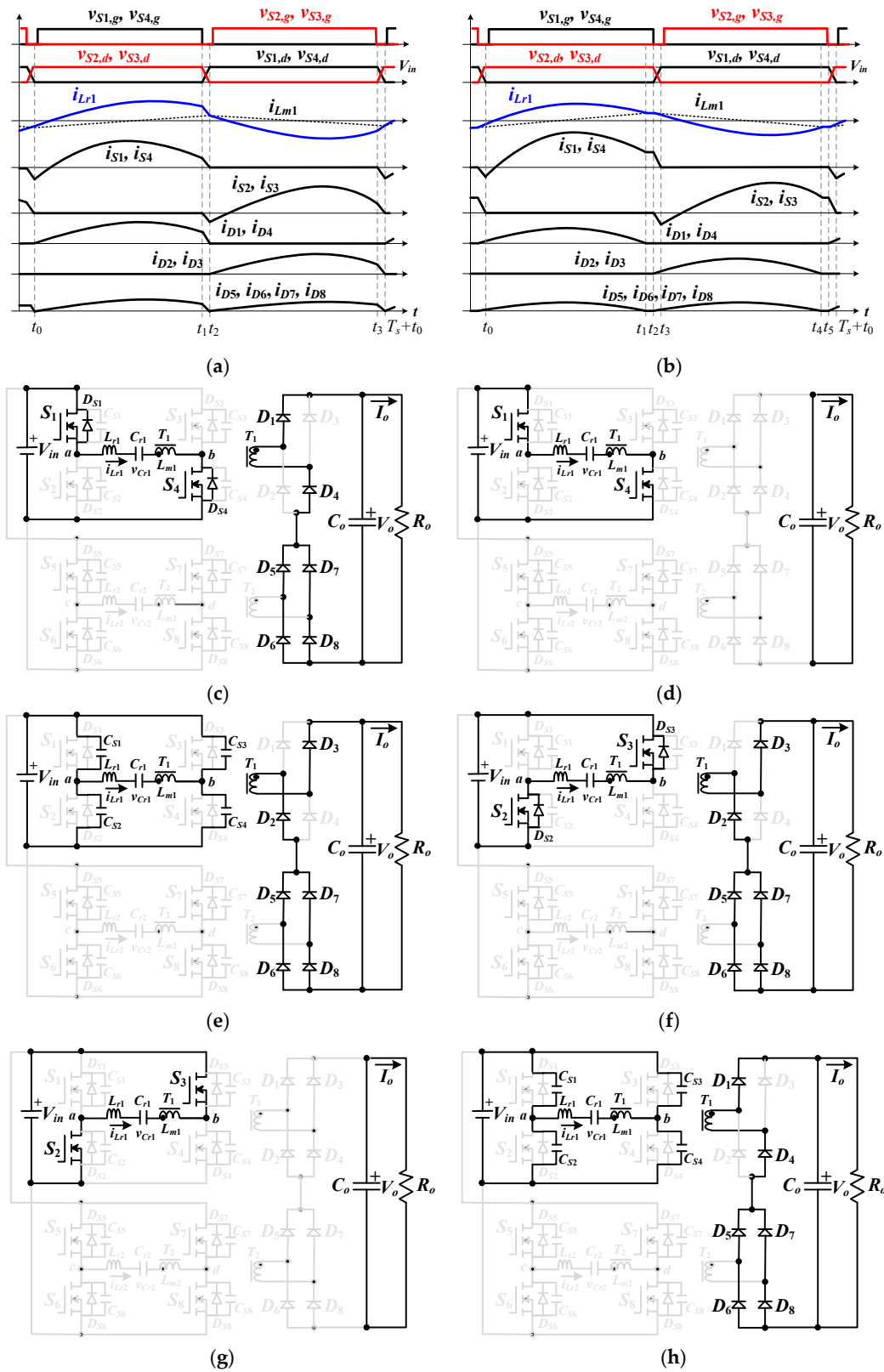


Figure 3. Circuit waveforms and equivalent mode circuits at low-voltage output. (a) PWM waveforms when $f_s > f_r$; (b) PWM waveforms when $f_s < f_r$; (c) mode 1; (d) mode 2; (e) mode 3; (f) mode 4; (g) mode 5; and (h) mode 6.

Mode 1 [t_0, t_1]: $S_1 \sim S_4$ are off and $i_{Lr1} < 0$ before time t_0 . C_{S1} and C_{S4} discharge by the current i_{Lr1} . At time t_0 , C_{S1} and C_{S4} discharge to zero voltage and D_{S1} and D_{S4} conduct. The drain-to-source voltages $v_{S1,d} = v_{S4,d} = 0$ and S_1 and S_4 turn on after t_0 under zero voltage condition. In mode 1, the load current flows through $D_1, C_o, R_o, D_5 \sim D_8$ and D_4 . The magnetizing inductor voltage $v_{Lm1} = nV_o$. C_{r1} and L_{r1} are naturally resonant with $v_{ab} = V_{in}$ and $v_{Lm1} = nV_o$. If $f_s < f_r$, then i_{D1}, i_{D4} , and $i_{D5} \sim i_{D8}$ will be reduced to zero before S_1 and S_4 turn off.

Mode 2 [t_1, t_2]: Due to $f_s < f_r$, $i_{Lm1} = i_{Lr1}$ at time t_1 so that $D_1 \sim D_8$ are off on the output side. L_{r1} , C_{r1} , and L_{m1} are naturally resonant with $V_{ab} = V_{in}$. If $f_s \approx f_r$, the peak-to-peak magnetizing current Δi_{Lm1} during one-half of switching period approximates:

$$\Delta i_{Lm1}(t) \approx \frac{nV_o}{2L_m f_s} \quad (4)$$

Mode 3 [t_2, t_3]: At time t_2 , S_1 and S_4 turn off. Owing to $i_{Lr1} > 0$, the voltages of C_{S2} and C_{S3} are decreased. If the current $i_{Lr1}(t_2) \approx \Delta i_{Lm1}/2$ is large enough, then the voltages of C_{S2} and C_{S3} will be decreased to zero at t_3 .

Mode 4 [t_3, t_4]: At t_3 , $v_{CS2} = v_{CS3} = 0$ and D_{S2} and D_{S3} conduct. S_2 and S_3 turn on after t_3 under zero voltage. The load current flows through $D_3, C_o, R_o, D_5 \sim D_8$, and D_2 so that $v_{Lm1} = -nV_o$. In mode 4, C_{r1} and L_{r1} are naturally resonant with $v_{ab} = -V_{in}$ and $v_{Lm1} = -nV_o$ in mode 4. If $f_s < f_r$, then i_{D2}, i_{D3} , and $i_{D5} \sim i_{D8}$ decrease to zero current before S_2 and S_3 turn off.

Mode 5 [t_4, t_5]: At t_4 , $i_{Lm1} = i_{Lr1}$ so that $D_1 \sim D_8$ are reverse biased. L_{r1}, C_{r1} , and L_{m1} are resonant with $v_{ab} = -V_{in}$. Mode 5 ends at t_5 when S_2 and S_3 turn off.

Mode 6 [$t_5, T_s + t_0$]: At t_5 , S_2 and S_3 turn off. Owing to $i_{Lr1} < 0$, C_{S1} and C_{S4} are discharged by i_{Lr1} . At time $T_s + t_0$, $v_{CS1} = v_{CS4} = 0$.

3. Circuit Characteristics and Design Guidelines

The load voltage control is based on the frequency modulation against line and load regulations. To ignore the harmonic components, the fundamental harmonic frequency approach is used to estimate the AC voltage gain of the studied circuit. The wide voltage operation is accomplished by selecting the series connections of two full-bridge diode rectifiers for high-voltage output (Figure 1a) or only one diode rectifier for low-voltage operation (Figure 1b). Since $S_1 \sim S_8$ have the $T_s/2$ turn-on time, the AC voltages v_{ab} and v_{cd} are square voltage waveforms with voltage values $\pm V_{in}$. The fundamental root-mean-square (*rms*) voltages $V_{ab,rms}$ and $V_{cd,rms}$ are calculated in Equation (5):

$$V_{ab,rms} = V_{cd,rms} = 2\sqrt{2}V_{in}/\pi \quad (5)$$

For high-voltage output, two full-bridge diode rectifiers are series-connected and connect to the output load. The magnetizing voltages $v_{Lm1} = v_{Lm2} = \pm nV_o/2$. For low-voltage output, only one full-bridge connects to the output load and the magnetizing voltage $v_{Lm1} = \pm nV_o$ and $v_{Lm2} = 0$. The fundamental *rms* magnetizing voltages $V_{Lm1,rms}$ and $V_{Lm2,rms}$ are calculated as:

$$V_{Lm1,rms} = \begin{cases} \sqrt{2}nV_{o,H}/\pi, & \text{for high voltage output} \\ 2\sqrt{2}nV_{o,L}/\pi, & \text{for low voltage output} \end{cases} \quad (6)$$

$$V_{Lm2,rms} = \begin{cases} \sqrt{2}nV_{o,H}/\pi, & \text{for high voltage output} \\ 0, & \text{for low voltage output} \end{cases} \quad (7)$$

where $V_{o,L}$ and $V_{o,H}$ denote the output voltage V_o at the low and high voltage ranges, respectively. From the given DC load resistor R_o , the equivalent primary side resistors R_{ac1} and R_{ac2} of T_1 and T_2 are calculated in Equations (8) and (9):

$$R_{ac1} = \begin{cases} \frac{4n^2 R_o}{\pi^2}, & \text{for high voltage output} \\ \frac{8n^2 R_o}{\pi^2}, & \text{for low voltage output} \end{cases} \quad (8)$$

$$R_{ac2} = \frac{4n^2 R_o}{\pi^2}, \text{ for high voltage output} \quad (9)$$

Based on the resonant circuit, the transfer function of the studied circuit is calculated in Equation (10):

$$|G| = \frac{V_{Lm1,rms}}{V_{ab,rms}} = \frac{1}{\sqrt{\left[1 + \frac{1}{l_n} \frac{f_n^2 - 1}{f_n^2}\right]^2 + x^2 \left(\frac{f_n^2 - 1}{f_n}\right)^2}} = \begin{cases} \frac{nV_{o,H}}{2V_{in}}, & \text{for high voltage output} \\ \frac{nV_{o,L}}{V_{in}}, & \text{for low voltage output} \end{cases} \quad (10)$$

where $f_n = f_s/f_r$ is the frequency ratio, $l_n = L_{m1}/L_{r1}$ is the inductor ratio, and $x = \sqrt{L_{r1}/C_{r1}}/R_{ac1}$ is the quality factor. The output voltage at high and low output voltage range can be re-written in Equations (11) and (12):

$$V_{o,H} = \frac{2V_{in}}{n \sqrt{\left[1 + \frac{1}{l_n} \frac{f_n^2 - 1}{f_n^2}\right]^2 + x^2 \left(\frac{f_n^2 - 1}{f_n}\right)^2}} \quad (11)$$

$$V_{o,L} = \frac{V_{in}}{n \sqrt{\left[1 + \frac{1}{l_n} \frac{f_n^2 - 1}{f_n^2}\right]^2 + x^2 \left(\frac{f_n^2 - 1}{f_n}\right)^2}} \quad (12)$$

Based on the output voltage range, $S_1 \sim S_8$ are regulated with variable frequency control to accomplish the wide voltage range output capability. Due to the resonant circuit always being controlled at the inductive impedance load, $S_1 \sim S_8$ will be operated under the soft switching condition.

To confirm the theoretical analysis, the design guideline of a laboratory circuit is provided. The electrical specifications of the prototype circuit are $V_{in} = 380$ V and $V_o = 110$ V~440 V (4:1 voltage ratio). The rated output power is 1000 W (200 W) for low (high)-voltage output and $f_r = 100$ kHz. To accomplish wide voltage output operation (4:1), two full-bridge resonant converters with input-parallel output-series connection are employed under the high output voltage range $V_{o,H} = 220$ V~440 V. However, only converter 1 is operated for low-voltage output $V_{o,L} = 110$ V~220 V. The voltage gain of the studied circuit with wide output voltage operation $V_o = 110$ V~440 V under the $V_{in} = 380$ V condition is provided in Figure 4. The transient voltage ($V_{o,tran}$) between two resonant converters' operation and one resonant converter operation is 220 V with ± 5 V voltage tolerance using a Schmitt trigger comparator, as shown in Figure 5. Since the voltage gain of the studied circuit in the low-voltage output range is two times the voltage gain in the high-voltage output range in Equation (10), two resonant converters' operation for high-voltage output (Figure 1a) and one resonant converter operation for low-voltage output (Figure 1b) have the same design procedure due to $V_{o,H} = 2V_{o,L}$ in Equations (11) and (12). Only one resonant converter is designed for the low-voltage output case to simplify the design guideline. For the low-voltage output case, the minimum voltage gain G_{min} is equal to unity at 110 V output voltage. The turns ratio n of T_1 can be obtained from Equation (13):

$$n = \frac{G_{min} V_{in}}{V_{o,L,min}} = \frac{1 \times 380 \text{ V}}{110 \text{ V}} \approx 3.455 \quad (13)$$

TDK (Tokyo Denki Kagaku, Tokyo, Japan) EE-55 magnetic cores with flux density $\Delta B = 0.4$ T and $A_e = 3.54$ cm² are adopted to implement transformers T_1 and T_2 . The minimum switching frequency

in the studied circuit is assumed at 60 kHz under $V_{o,tran}$ output. The minimum primary winding turns are obtained in Equation (14):

$$N_{p1,min} \geq \frac{nV_{o,tran}}{2f_{s,min}\Delta BA_e} = \frac{3.455 \times 220 \text{ V}}{2 \times 60000 \text{ Hz} \times 0.4 \text{ T} \times 3.54 \times 10^{-4} \text{ m}^2} \approx 45 \quad (14)$$

In the prototype circuit, the actual transformer winding turns of T_1 and T_2 are $N_{p1} = N_{p2} = 45$ and $N_{s1} = N_{s2} = 13$. The equivalent primary side resistance R_{ac1} under $P_{o,max} = 1000 \text{ W}$ and $V_{o,L,min} = 110 \text{ V}$ is calculated in Equation (15):

$$R_{ac1} = \frac{8n^2}{\pi^2} R_{o,rated} = \frac{8 \times (45/13)^2}{\pi^2} \times \frac{(110 \text{ V})^2}{1000 \text{ W}} \approx 117.5 \Omega \quad (15)$$

In the prototype circuit, the selected parameters $l_n = 5$ and $x = 0.2$. The resonant components L_{r1} , L_{r2} , L_{m1} , L_{m2} , C_{r1} , and C_{r2} are calculated as:

$$L_{r1} = L_{r2} = \frac{xR_{ac1}}{2\pi f_r} = \frac{0.2 \times 117.5 \Omega}{2\pi \times 100 \times 10^3 \text{ Hz}} \approx 37.4 \mu\text{H} \quad (16)$$

$$L_{m1} = L_{m2} = l_n L_{r1} = 37.4 \times 5 \mu\text{H} = 187 \mu\text{H} \quad (17)$$

$$C_{r1} = C_{r2} = \frac{1}{4\pi^2 L_{r1} f_r^2} = \frac{1}{4\pi^2 \times 37.4 \times 10^{-6} \text{ F} \times (100 \times 10^3 \text{ Hz})^2} \approx 68 \text{ nF} \quad (18)$$

The voltage ratings of $D_1 \sim D_8$ are equal to $V_{o,max}/2 = 220 \text{ V}$. The voltage ratings of $S_1 \sim S_8$ are $V_{in} = 380 \text{ V}$. Power switches SiHG20N50C (500 V/ 11A) are employed for $S_1 \sim S_8$ and SBR20A300CTFP (300 V/20 A) are used for $D_1 \sim D_8$. The selected output capacitance $C_o = 720 \mu\text{F}/450 \text{ V}$. The frequency modulation controller UCC25600 is adopted to generate the gating signals of $S_1 \sim S_8$.

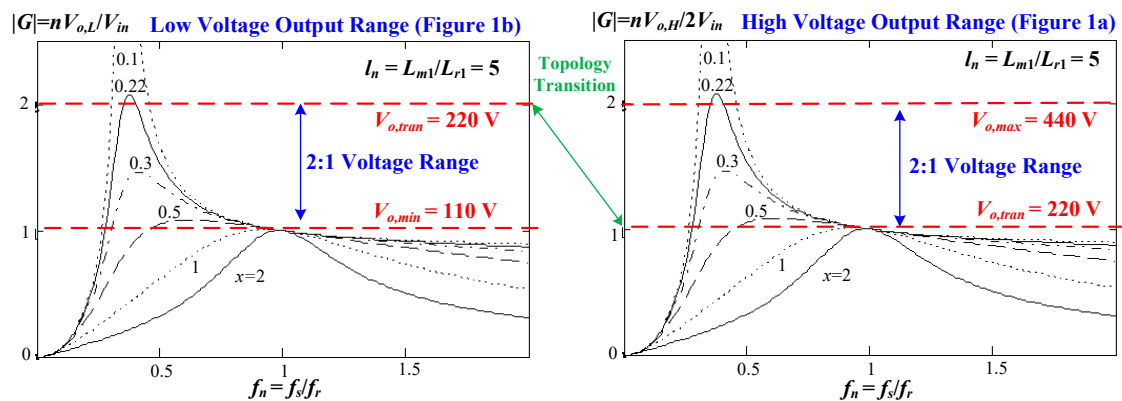


Figure 4. Gain curves of the studied circuit with output voltage $V_o = 110 \text{ V} \sim 440 \text{ V}$ and input voltage $V_{in} = 380 \text{ V}$.

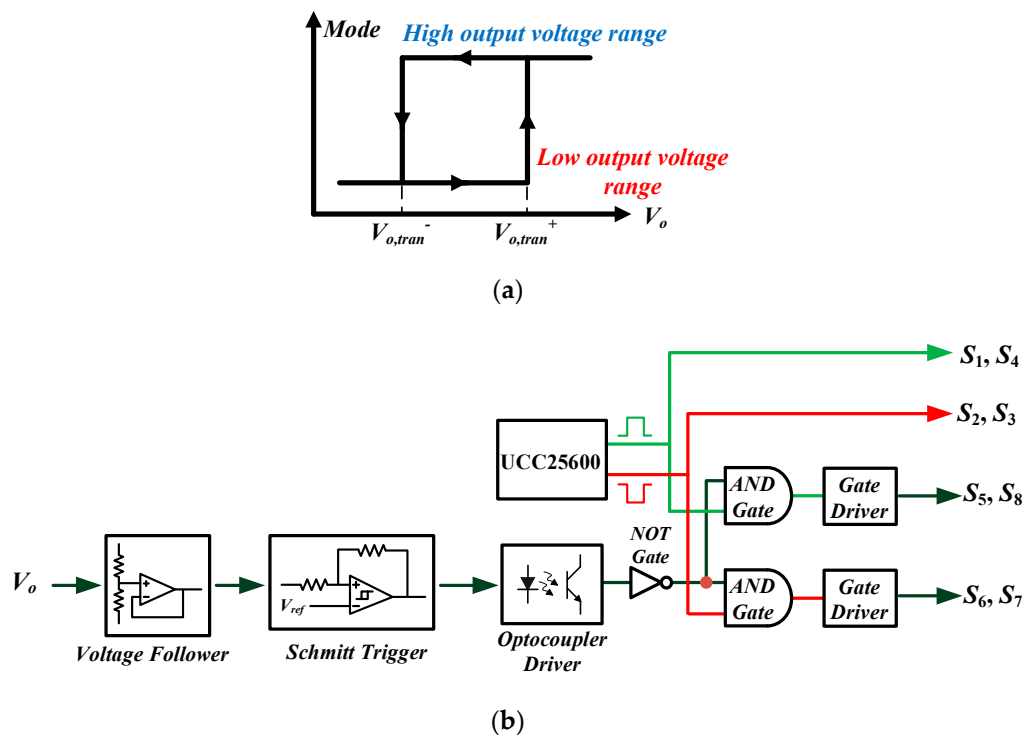


Figure 5. Control block of voltage transition operation. (a) Schmitt comparator; and (b) control block of signals $S_1 \sim S_8$.

4. Experimental Verification

A laboratory prototype (Figure 6) was constructed and tested. The circuit parameters are calculated from the previous section. The test waveforms are demonstrated and shown to confirm the theoretical discussion and effectiveness of the studied circuit with a wide output voltage range. Figures 7 and 8 provide the experimental results under low-voltage range with only one resonant converter operation. Figure 7 demonstrates the experimental waveforms for $V_o = 110$ V and $P_o = 1$ kW. The experimental waveforms of $v_{S1,g} \sim v_{S4,g}$ are given in Figure 7a. The switching frequency of $S_1 \sim S_4$ is about 100 kHz. The leg voltage v_{ab} and the resonant component waveforms v_{Cr1} and i_{Lr1} are provided in Figure 7b. v_{Cr1} and i_{Lr1} are almost sinusoidal waveforms due to $f_s \approx f_r$. The inductor current i_{Lr1} is lagging to the measured voltage v_{ab} . The input impedance of the resonant tank by C_{r1} , L_{r1} , L_{m1} , and R_{ac1} is operated at the inductive load. Figure 7c,d provide the measured diode currents. It is obvious that $D_1 \sim D_4$ turn off under zero current. There is a slight current imbalance on D_5 and D_7 due to the unequal PCB layout length of D_5 and D_7 . Figure 7e provides the test results of V_{in} , V_o , and I_o . The output voltage V_o is controlled at 110 V output and the load current is 9.1 A. Figure 7f shows the experimental waveforms $v_{S1,g}$, $v_{S1,d}$, and i_{S1} . It is observed that the drain voltage $v_{S1,d}$ is decreased to zero before S_1 turns on. The zero-voltage turn-on switching of switch S_1 is achieved in Figure 7f. $S_2 \sim S_4$ have the same turn-on characteristic as S_1 . It can be expected that the zero-voltage turn-on switching of $S_2 \sim S_4$ is also implemented.

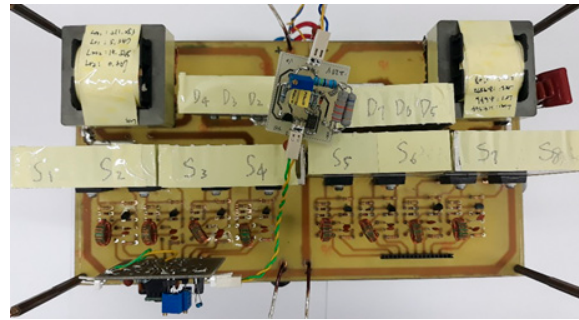


Figure 6. Picture of the proposed converter.

Figure 8 provides the measured results for $V_o = 215$ V and $P_o = 1$ kW. The experimental waveforms $v_{S1,g} \sim v_{S4,g}$ are given in Figure 8a and the switching frequency is about 57 kHz. Comparing the test results in Figures 7a and 8a, the switching frequency under $V_o = 215$ V is lower than the switching frequency under the $V_o = 110$ V case. Figure 8b illustrates the measured signals of v_{ab} , v_{Cr1} , and i_{Lr1} . i_{Lr1} is a quasi-sinusoidal waveform due to $f_s < f_r$ under $V_o = 215$ V. The inductor current i_{Lr1} is lagging the measured voltage v_{ab} . The input impedance of the resonant tank by C_{r1} , L_{r1} , L_{m1} , and R_{ac1} is operated at the inductive load. The measured diode currents on the output side are provided in Figure 8c,d. It can be observed that $D_1 \sim D_4$ turns off under zero current. The measured waveforms of V_{in} , V_o , and I_o are provided in Figure 8e. Figure 8f shows the experimental waveforms $v_{S1,g}$, $v_{S1,d}$, and i_{S1} . It is clear that $v_{S1,d}$ is decreased to zero before S_1 turns on. The zero-voltage turn-on switching of S_1 is achieved in Figure 8f for $V_o = 215$ V condition.

Figures 9 and 10 give the measured waveforms for the high-voltage output range. Two full-bridge resonant converters with primary-parallel secondary-series connection are controlled in the presented converter to provide high-voltage output. Figure 9 provides the experimental results at $V_o = 225$ V and $P_o = 2000$ W. Figure 10 gives the experimental waveforms at 440 V output voltage and 2 kW output power. Figure 9a,b provide the waveforms of $S_1 \sim S_8$ and the switching frequency is about 106 kHz. Figure 9c provides the capacitor voltages and inductor currents of two full-bridge resonant converters. The voltage and current waveforms on two full-bridge circuits are balanced well. The measured diode currents on the secondary sides are demonstrated in Figure 9d,e and the diode currents $i_{D1} \sim i_{D8}$ of two full-bridge diode rectifiers are also balanced well. Figure 9f provides the measured results of V_{in} , V_o , and I_o . The measured voltage $V_o = 225$ V and $I_o = 8.8$ A. The experimental waveforms $v_{S1,g}$, $v_{S1,d}$, and i_{S1} are given in Figure 9g. Before S_1 is turned on, $v_{S1,d}$ is decreased to zero. The soft switching turn-on of S_1 is realized for $V_o = 225$ V case. The switch signals $S_1 \sim S_4$ and $S_5 \sim S_8$ are demonstrated in Figure 10a,b under $V_o = 440$ V and $P_o = 2$ kW conditions. The switching frequency is about 59 kHz. The experimental results of v_{Cr1} , v_{Cr2} , i_{Lr1} , and i_{Lr2} are shown in Figure 10c. It is clear that capacitor voltages v_{Cr1} and v_{Cr2} and inductor currents i_{Lr1} and i_{Lr2} , i_{Lr1} , and i_{Lr} are well balanced. The diode currents $i_{D1} \sim i_{D4}$ and $i_{D5} \sim i_{D8}$ are provided in Figure 10d,e, respectively. It can be observed that $i_{D1} \sim i_{D4}$ and $i_{D5} \sim i_{D8}$ are well balanced. The measured waveforms of V_{in} , V_o , and I_o are provided in Figure 10f under $V_o = 440$ V and $I_o = 4.6$ A. The experimental waveforms $v_{S1,g}$, $v_{S1,d}$, and i_{S1} are given in Figure 10g. Before S_1 is turned on, the drain voltage $v_{S1,d}$ has been decreased to zero. The soft switching turn-on of S_1 is achieved for the $V_o = 400$ V case.

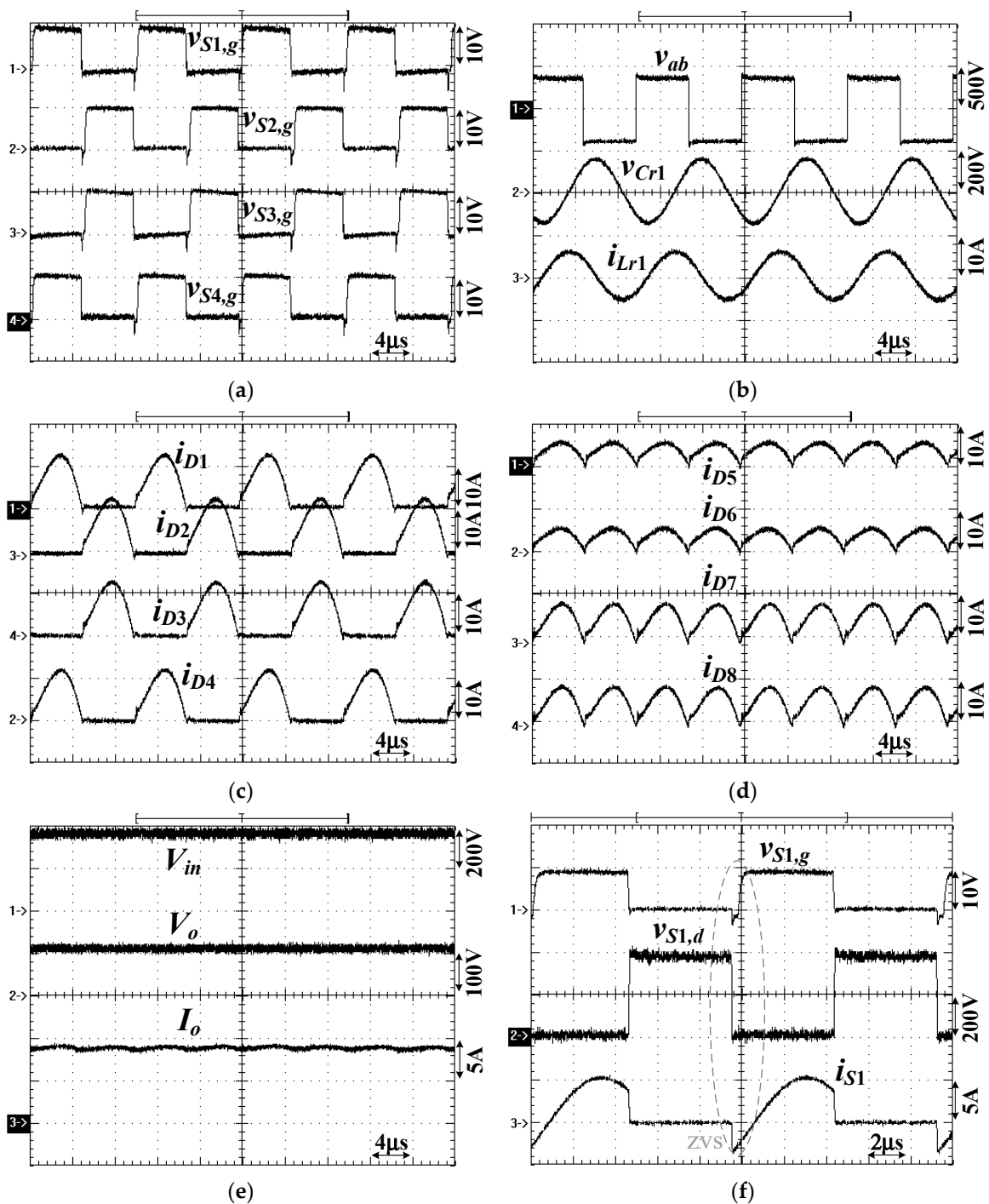


Figure 7. Measured results at 110 V output and 1 kW load under the low output voltage range. (a) PWM signals $v_{S1,g} \sim v_{S4,g}$; (b) v_{ab} , v_{Cr1} , i_{Lr1} ; (c) diode currents $i_{D1} \sim i_{D4}$; (d) diode currents $i_{D5} \sim i_{D8}$; (e) V_{in} , V_o , I_o ; and (f) $v_{S1,g}$, $v_{S1,d}$, i_{S1} .

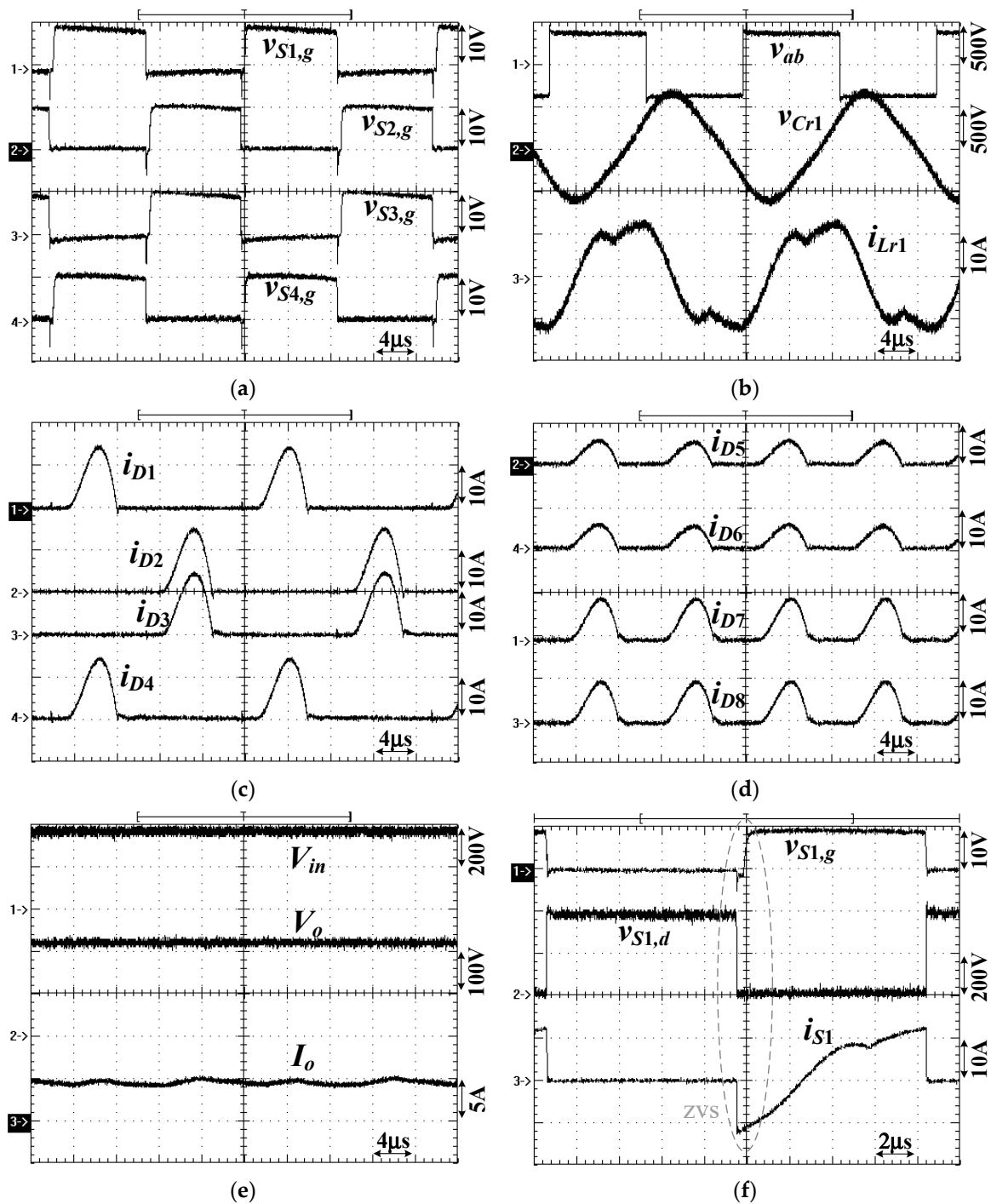


Figure 8. Measured results at 215 V output and 1 kW load under the low output voltage range. (a) PWM signals $v_{S1,g} \sim v_{S4,g}$; (b) v_{ab} , v_{Cr1} , i_{Lr1} ; (c) diode currents $i_{D1} \sim i_{D4}$; (d) diode currents $i_{D5} \sim i_{D8}$; (e) V_{in} , V_o , I_o ; and (f) $v_{S1,g}$, $v_{S1,d}$, i_{S1} .

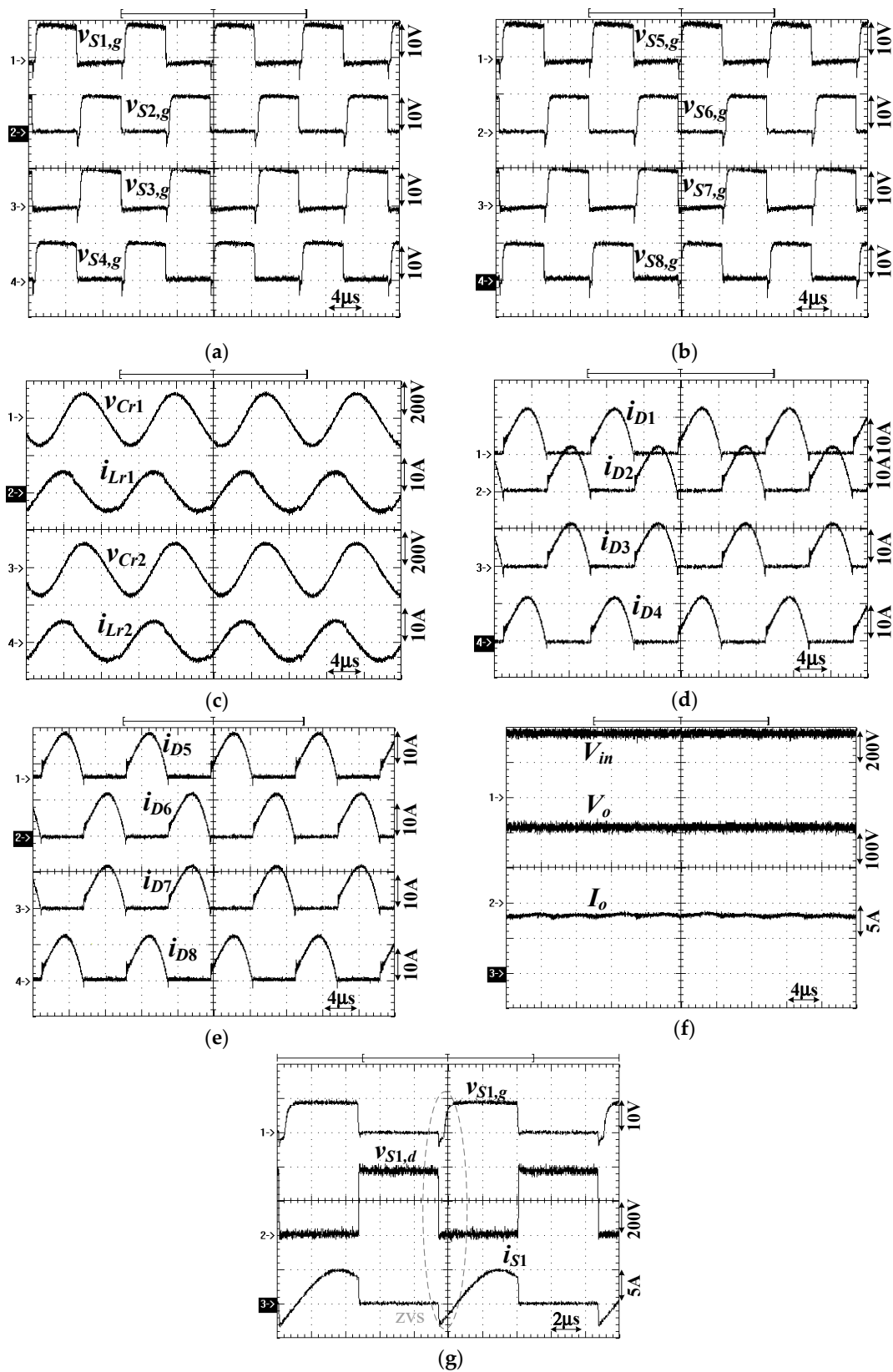


Figure 9. Measured results at 225 V output and 2 kW load under the high output voltage range. (a) PWM signals $v_{S1,g} \sim v_{S4,g}$; (b) PWM signals $v_{S5,g} \sim v_{S8,g}$; (c) v_{Cr1} , i_{Lr1} , v_{Cr2} , i_{Lr2} ; (d) diode currents $i_{D1} \sim i_{D4}$; (e) diode currents $i_{D5} \sim i_{D8}$; (f) V_{in} , V_o , I_o ; and (g) $v_{S1,g}$, $v_{S1,d}$, i_{S1} .

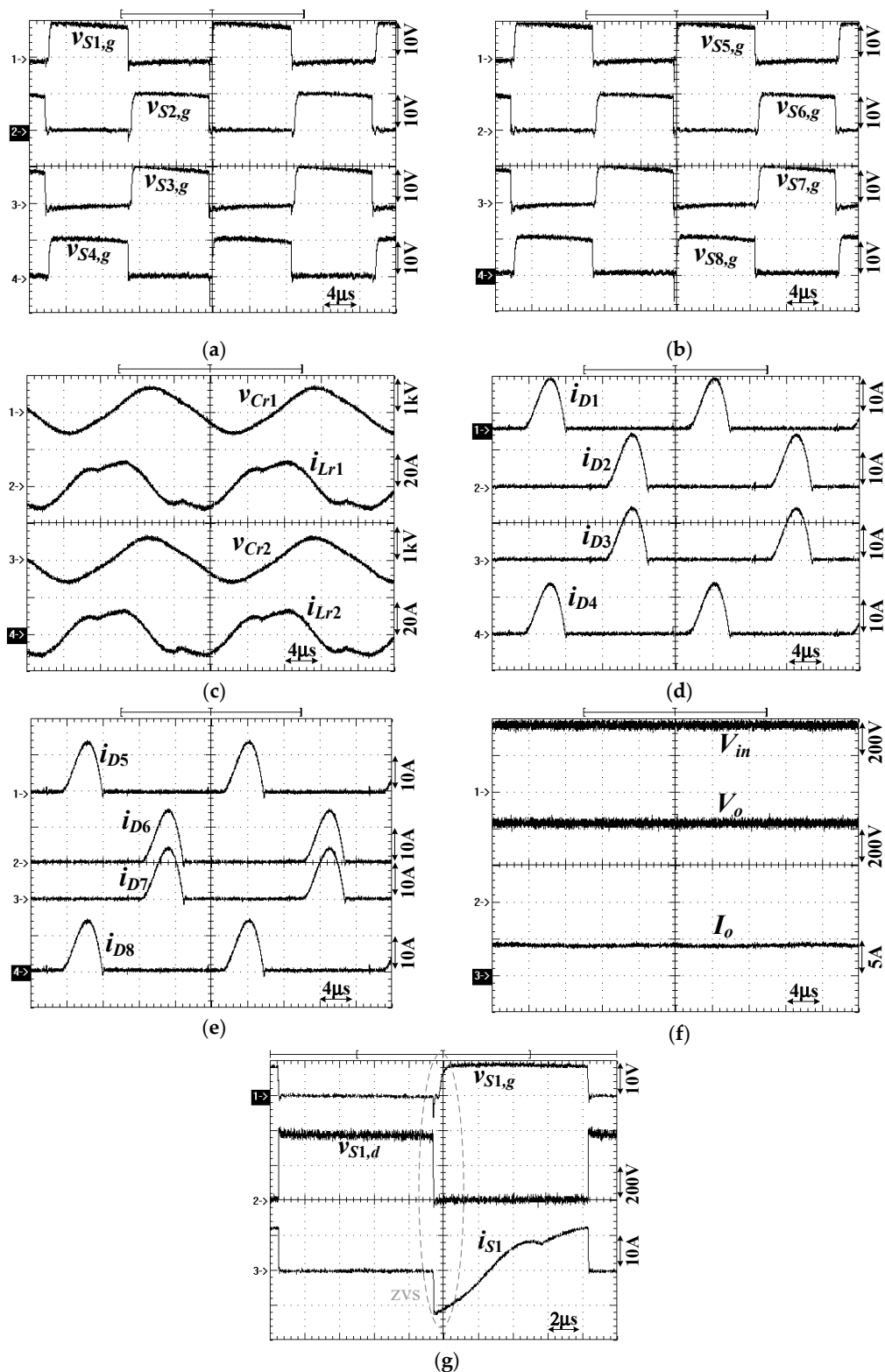


Figure 10. Measured results at 440 V output and 2 kW load under a high output voltage range. (a) PWM signals $v_{S1,g}$ ~ $v_{S4,g}$; (b) PWM signals $v_{S5,g}$ ~ $v_{S8,g}$; (c) v_{Cr1} , i_{Lr1} , v_{Cr2} , i_{Lr2} ; (d) diode currents i_{D1} ~ i_{D4} ; (e) diode currents i_{D5} ~ i_{D8} ; (f) V_{in} , V_o , I_o ; and (g) $v_{S1,g}$, $v_{S1,d}$, i_{S1} .

Figure 11 shows the measured efficiencies of the proposed converter under different output voltages and rated power. The test efficiencies of the presented circuit are 94.4% at $V_o = 110$ V under $P_o = 1$ kW (low output voltage range), 90.1% at $V_o = 215$ V under $P_o = 1$ kW (low output voltage

range), 96.7% at $V_o = 225$ V under $P_o = 2$ kW (high output voltage range) and 90.6% at $V_o = 440$ V under $P_o = 1$ kW (high output voltage range). From the test results, it can be observed that the circuit efficiency in the low-voltage case $V_o = 110$ V ($V_o = 225$ V) is better than the high-voltage case $V_o = 215$ V ($V_o = 440$ V) for low output voltage range (high output voltage range). The switching period at $V_o = 215$ V is greater than the switching period at $V_o = 110$ V. Due to the magnetizing current loss, which depended on the output voltage and the switching period, the estimated power loss from the magnetizing current at $V_o = 215$ V output is greater than the $V_o = 110$ V case. Therefore, the measured efficiency of the studied converter at $V_o = 110$ V is better than the $V_o = 215$ V output. Similarly, the measured circuit efficiency at $V_o = 225$ V is better than the $V_o = 440$ V output. Comparing the circuits shown in Figure 1, it can be observed that one full-bridge resonant converter and eight rectifier diodes are operated for the low-voltage output case, and two full-bridge resonant converters and eight rectifier diodes are operated for the high-voltage output case. It is clear that there are more conduction losses on diodes $D_5 \sim D_8$ for the low-voltage output. The power losses on these diodes are equal to $2V_f I_o$, where V_f is the voltage drop on $D_5 \sim D_8$. The percentage between the power loss on diodes $D_5 \sim D_8$ and the rated power is about $2V_f/V_o$. Since $V_o \gg V_f$, it can be expected that this extra power loss on diodes $D_5 \sim D_8$ will not result in serious problems. Due to the $V_f = 0.9$ V for diodes SBR20A300CTFP, the calculated power loss percentage on diodes $D_5 \sim D_8$ is about 1.6% in the 110 V output case and 0.8% in the 215 V output case.

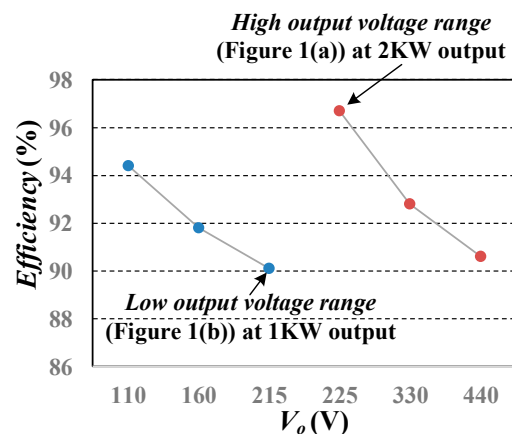


Figure 11. Measured circuit efficiencies of the proposed converter under different output voltages and the rated power.

5. Conclusions

A new resonant circuit with a series-parallel structure is presented in this paper to achieve the benefits of low switching loss, wide output voltage capability, and low-voltage rating on rectifier diodes. In the proposed converter, two diode rectifiers with series-connection are employed on the secondary side to reduce the voltage rating on the rectifier diodes for high output voltage range operation. The voltage rating of rectifier diodes is $V_{o,max}/2$ instead of the $V_{o,max}$ voltage rating in conventional resonant converters. Since the proposed resonant tank is operated under the inductive load condition, the soft switching operation can be implemented in the studied converter. Finally, a 2 kW laboratory circuit was constructed and experiments are demonstrated to confirm the usefulness of the presented hybrid resonant converter for wide voltage output capability.

Author Contributions: B.-R.L. proposed and designed this project and was responsible for writing the paper.

Funding: This research is funded by the Ministry of Science and Technology, Taiwan, under grant number MOST 108-2221-E-224-022-MY2.

Acknowledgments: This research is supported by the Ministry of Science and Technology, Taiwan, under contract MOST 108-2221-E-224-022-MY2. The author would like to thank Mr. H. R. Cheng for his help to measure the circuit waveforms in the experiment.

Conflicts of Interest: The author declares no potential conflict of interest.

References

1. Wang, Y.; Zhang, S.; Guan, Y.; Liu, X.; Xu, D. Single-stage QR ac-dc converter based on buck-boost and flyback circuits. *IET Power Electron.* **2017**, *10*, 103–111. [[CrossRef](#)]
2. Xie, X.; Li, J.; Peng, K.; Zhao, C.; Lu, Q. Study on the single-stage forward-flyback PFC converter with QR control. *IEEE Trans. Power Electron.* **2016**, *31*, 430–442. [[CrossRef](#)]
3. Lin, B.R.; Chiang, H.K.; Chen, C.C. Analysis and implementation of a zvs-pwm converter with series-connected transformers. *IEEE Trans. Circuits Syst. II* **2007**, *54*, 917–921. [[CrossRef](#)]
4. Singh, A.K.; Das, P.; Panda, S.K. Analysis and design of SQR-based high-voltage LLC resonant dc-dc converter. *IEEE Trans. Power Electron.* **2017**, *32*, 4466–4481. [[CrossRef](#)]
5. Haga, H.; Kurokawa, F. Modulation method of a full-bridge three-level LLC resonant converter for battery charger of electric vehicles. *IEEE Trans. Power Electron.* **2017**, *32*, 2498–2507. [[CrossRef](#)]
6. Steigerwald, R.L. A comparison of half-bridge resonant converter topologies. *IEEE Trans. Power Electron.* **1988**, *3*, 174–182. [[CrossRef](#)]
7. Lin, B.R.; Lin, Y. Parallel current-fed resonant converter with balance current sharing and no input ripple current. *IET Power Electron.* **2019**, *12*, 212–219. [[CrossRef](#)]
8. Safaee, A.; Jain, P.; Bakhshai, A. A ZVS pulsewidth modulation full-bridge converter with a low-RMS-current resonant auxiliary circuit. *IEEE Trans. Power Electron.* **2016**, *31*, 4031–4047. [[CrossRef](#)]
9. Liu, P.J.; Hsu, Y.C.; Hsu, S.R. Drain-voltage balance and phase-shifted PWM control schemes for high-efficiency parallel-string dimmable LED drivers. *IEEE Trans. Ind. Electron.* **2018**, *65*, 6168–6176. [[CrossRef](#)]
10. Lee, I.O.; Moon, G.W. Phase-shifted PWM converter with a wide ZVS range and reduced circulating current. *IEEE Trans. Power Electron.* **2013**, *28*, 908–919. [[CrossRef](#)]
11. Mishima, T.; Akamatsu, K.; Nakaoka, M. A high frequency-link secondary-side phase-shifted full-bridge soft-switching PWM DC-DC converter with ZCS active rectifier for EV battery charged. *IEEE Trans. Power Electron.* **2013**, *28*, 5758–5773. [[CrossRef](#)]
12. Li, Z.; Wu, T.; Zhang, G.; Yang, R. High modulation method combining variable frequency and double phase-shift for a 10 kW LLC resonant converter. *IET Power Electron.* **2018**, *11*, 2161–2169. [[CrossRef](#)]
13. Pahlevani, M.; Pan, S.; Jain, P. A hybrid phase-shift modulation technique for DC/DC converters with a wide range of operating conditions. *IEEE Trans. Ind. Electron.* **2016**, *63*, 7498–7510. [[CrossRef](#)]
14. Jovanović, M.M.; Irving, B.T. On the fly topology-morphing control efficiency optimization method for LLC resonant converters operating in wide input and/or output-voltage range. *IEEE Trans. Power Electron.* **2016**, *31*, 2596–2608. [[CrossRef](#)]
15. Zhang, C.; Gao, Z.; Liao, X. Bidirectional dc-dc converter with series-connected resonant tanks to realize soft switching. *IET Power Electron.* **2018**, *11*, 2029–2043. [[CrossRef](#)]
16. Sun, W.; Xing, Y.; Wu, H.; Ding, J. Modified high-efficiency LLC converters with two split resonant branches for wide input-voltage range applications. *IEEE Trans. Power Electron.* **2018**, *33*, 7867–7870. [[CrossRef](#)]



© 2019 by the author. Licensee MDPI, Basel, Switzerland. This article is an open access article distributed under the terms and conditions of the Creative Commons Attribution (CC BY) license (<http://creativecommons.org/licenses/by/4.0/>).